

Manoeuvring Simulations of Autonomous Underwater Vehicle using Quaternion

Prasad Vinayak Patil,[§] Md. Kareem Khan,[#] Manu Korulla,[#] Vishwanath Nagarajan,^{§,*} and Om Prakash Sha[§]

[§]Indian Institute of Technology Kharagpur, India

[#]Naval Science & Technological Laboratory, India

*Email: vishwanath_n@naval.iitkgp.ac.in

ABSTRACT

The dynamics of an AUV, which can perform manoeuvres with pitch angles in the range of 90° is investigated in this paper. The purpose of the AUV is to perform a station-keeping manoeuvre at about 90° pitch angle by varying propeller revolution. The AUV is launched in horizontal orientation. Quaternion mathematics, 4 quadrant propeller open water characteristics, and PID controller for propeller revolution are incorporated in manoeuvring mathematical model for this purpose. A procedure for optimizing the gain coefficients for the PID controller is developed using the 7 DoF manoeuvring mathematical model. Two design configurations of the AUV are investigated, positively buoyant and negatively buoyant. The design objective is, the AUV shall travel as far away as possible from the parent vehicle using minimum energy and time. It is shown that both the optimal gain coefficients for the PID controller for propeller revolution and the dynamic response of the AUV is different for each design configuration. The methodology developed in the paper can be used in the design and propeller revolution control system for certain categories of AUVs. The study shows that prime mover torque/ shaft revolution and 7 DoF manoeuvring mathematical model are important in predicting the attitude and trajectory in space and station-keeping manoeuvring capability of an AUV launched from a parent vehicle.

Keywords: AUV; Quaternion; 4 quadrant propeller operation; Station-keeping

NOMENCLATURE

A_F	Area of stern plane	w_F	Wake coefficient at stern plane position
A_R	Area of rudder	w_P	Wake coefficient at propeller position in manoeuvring motions
a_H	Ratio of additional lateral force induced on ship hull by rudder action to the rudder force	w_{P0}	Wake coefficient at propeller position in straight moving
B	Buoyancy	w_R	Wake coefficient at rudder position
C_B	Block coefficient	W	Weight of AUV (= mg)
C_D	Drag coefficient	Z_0	Launch depth
C_T, C_Q, C_{TN}	Four quadrant propeller thrust, torque, duct thrust coefficient	Z_d	Station-keeping depth
$C_F(\lambda_F)$	Slope of stern plane normal force coefficient	Z_e	Manoeuvring depth of AUV from water surface
$C_R(\lambda_R)$	Slope of rudder normal force coefficient	Z_{pr}	Number of blades (propeller)
D	Diameter of AUV	z'_p	Z coordinate of propeller position / L

D_E	Distance travelled by AUV	α	Angle of attack
D_P	Diameter of propeller	α_F, α_R	Effective inflow angle to stern plane and rudder respectively
F_n	Froude number	β	Drift angle
I_{PP}	Mass moment of rotary inertia of propeller	β_a	Hydrodynamic pitch angle at $0.35 D_p$ radial section
ΔI_{PP}	Added mass moment of rotary inertia of propeller	γ_R	Flow straightening coefficient
J	Propeller advance ratio	δ_F	Stern plane angle
K_H, M_H, N_H	X, Y, Z hull moments	δ_R	Rudder angle
K_T, K_Q, K_{TD}	Propeller open water thrust, torque and duct thrust coefficients	η_M	Electric motor efficiency
K_{XX}, K_{YY}, K_{ZZ}	Radii of gyration of AUV about its X, Y and Z axis respectively	η_R	Relative rotative efficiency
L	Length of AUV	η_S	Shafting efficiency
m	Mass of AUV	ϕ, θ, ψ	Euler angles in the sequence roll, pitch, and yaw angle when rotating from body fixed to Earth axis
M_P	Mass of the propeller	λ_F, λ_R	Aspect ratio of a stern plane and rudder respectively
n	Propeller revolution	ρ	density of water
n_{\max}	Maximum propeller revolution limit		
p, q, r	AUV's roll, pitch and yaw rate		$\text{Energy}' = \frac{\text{Energy}}{0.5 * \rho * U_0^2 * L^3}$ $Fn = \sqrt{g * L}$
P / D_p	Propeller pitch to diameter ratio		$M' = \frac{M_H}{0.5 * \rho * L^3 * U_0^2}$ $n'_{\max} = n_{\max} * L / U_0$
Q_E	Prime mover torque		
Q_P	Propeller torque		$p' = p * L / U_0, q' = q * L / U_0,$ $r' = r * L / U_0$
t_p	Thrust deduction factor		$\text{Power}' = \frac{\text{Power}}{0.5 * \rho * U_0^3 * L^2}$
U_0	Launch speed		$Q_E' = \frac{Q_E}{0.5 * \rho * U_0^2 * L^3}$
U_F, U_R	Effective inflow velocity to a stern plane and rudder respectively		$Q_P' = \frac{Q_P}{0.5 * \rho * U_0^2 * L^3}$
u, v, w	AUV's surge, sway, heave velocity		$R_T' = \frac{R_T}{0.5 * \rho * L^2 * U_0^2}$
X_E, Y_E, Z_E	X, Y, Z coordinates in ECEF frame		$rps' = rps * L / U_0$

X_H, Y_H, Z_H	X, Y, Z Hull forces
X_P, Y_P, Z_P	Propeller force in surge, sway, heave direction
X_R, Y_R, Z_R	Rudder force in surge, sway, heave direction
x_B, y_B, z_B	Coordinates of centre of buoyancy of AUV
x_G, y_G, z_G	Coordinates of centre of mass of AUV
x'_p	X coordinate of propeller position / L

$$time' = U_0 * time / L$$

$$u' = u / U_0, v' = v / U_0, w' = w / U_0$$

$$X' = \frac{X_H}{0.5 * \rho * L^2 * U_0^2}$$

$$X_P' = \frac{X_P}{0.5 * \rho * U_0^2 * L^2}$$

$$Z' = \frac{Z_H}{0.5 * \rho * L^2 * U_0^2}$$

$$Z'_e = Z_e / L$$

1. INTRODUCTION

In many countries, research on underwater robots has become a topic of considerable interest. Autonomous Underwater Vehicle (AUV) can perform tasks such as ocean exploration, observation, detection, and salvage. AUVs not only substitute risky underwater work usually undertaken by people but also conduct comprehensive exploration as well as exploration at depths that cannot be achieved by ordinary diving technology. Li¹ *et al.* demonstrated the constructions of the AUV and its three core modules - vision module, navigation module, and control module. They have tested the AUV for mobility in the vertical as well as horizontal planes. Song² *et al.* investigated stable navigation of negative-buoyancy autorotating-rotor AUV. He concluded that the negative-buoyancy autorotating-rotor AUV has a greater carrying capacity and better applicability than the neutral buoyancy vehicle. Rezazadegan³ *et al.* carried out trajectory tracking control of an underactuated AUV in 6 degree of freedom (DoF) by assuming the system parameters are unknown. They showed that a nonlinear adaptive control scheme yields asymptotic convergence of the AUV to the reference trajectory, in the presence of parametric uncertainties. The stability of the presented control laws is demonstrated and its efficiency is shown using saturation functions by numerical simulations. Ayyangar⁴ *et al.* carried out a stability analysis of a slow-moving positively buoyant AUV in the vertical plane for a level flight at varying buoyancy and speeds are studied to show a steady-depth path is achieved by the balance of the restoring, control, and damping force. They showed that the stability changes from oscillatory to a steady node at a transition speed that depends on the metacentric height. It was also shown that the positive buoyancy has a marginal effect on the transition speed but influences the stern plane angles and pitch of the vehicle. Rodriguez⁵ *et al.* investigated micro autonomous underwater hovering vehicle-ship interactions in terms of hydrodynamic interaction, seakeeping performance for communication, launch, and recovery near a free surface. The modelling of an AUV using quaternion formulation for angular position description and Lagrange method to compute the equations of motion is discussed. They showed that when the vehicle follows a sequence of way-points including vertical diving motion, their proposed guidance algorithm and motion control are relevant both in terms of effectiveness and robustness

for this particular type of vehicle and orientation formulation. Ferreira⁶ *et al.* investigated the control of a nonholonomic AUV in the 3D space. They showed that the dynamics of the AUV is nonlinear. Therefore, different controllers based on Lyapunov theory are proposed. The performance of controllers is verified using simulations and experiments. Ferreira⁷ *et al.* further investigated an approach to control a 4 DoF AUV in the vertical and the horizontal planes while pitching bow up or down by 90°. They showed that although roll angle is not controllable, their proposed guidance law is able to manoeuvre the AUV to any point in the horizontal plane while maintaining the AUV in a vertical position. Chen⁸ *et al.* developed manoeuvring models and systems of a simulator to improve the motion performance of AUVs at the preliminary design stage. The computational results from the proposed simulator agreed well with those from both the model AUV experiments and the Euler-angle based simulations. A new manoeuvring procedure, namely “put-out”, was implemented to test the directional stability of an AUV in the proposed AUV simulator that can be considered for vehicles in space as well as in constrained planes. Fjellstad and Fossen⁹ applied position and attitude set-point regulation of AUVs in 6 DoF. Euler parameters are used in the representation of global attitude. Non-linear PD-control law is derived by using a general Lyapunov function for the 6 DoF dynamic model of the AUV. Excellent performance of the control law for an AUV in 6 DoF is demonstrated by simulations.

Andersen and Kristiansen¹⁰ investigated 3D guidance strategy for fixed-wing unmanned aerial vehicle (UAV) using quaternions. The algorithm is based on constructing two quaternions, one which makes the UAV fly towards the path and one that makes the UAV follow the path. These two quaternions are then blended such that the path-following objective is reached. The guidance algorithm is applied to a kinematic model for a fixed-wing UAV with a kinematic controller and its performance were verified by numerical simulations. Chen¹¹ *et al.* analyse the nonholonomic characteristics, constraint non-integrability, and controllability of UAVs to realize the three-dimensional stabilization control of fixed-wing UAVs with continuous feedback controller. They designed a continuous periodic time-varying controller, which can cause a UAV to exponentially converge to the origin; when

the track deviates, the UAV can rapidly return to the original track. Wang and Liu¹² studied the trajectory tracking control problem of a 6 DoF quadrotor UAV with input saturation. They achieved globally uniformly ultimately bounded stability of the closed-loop system with the proposed control scheme by avoiding the latent singularities in the attitude extraction process caused by saturation nonlinearities. Li¹³ *et al.* analysed nonlinear characteristics of underactuated AUVs based on the Taylor series. Based on the nonlinear characteristics of an underactuated AUV, quaternion theory was applied to transfer the underactuated AUV motion function to develop a time-varying control law. This control law achieved a stabilization in arbitrary initial positions. Lekkas and Fossen¹⁴ presented a quaternion version of the Line-of-Sight (LOS) guidance algorithm for a 5 DoF torpedo-shaped AUV model neglecting roll angle. The proposed method provides a singularity-free and computationally efficient version of the conventional LOS algorithm. Gavrilina and Chestnov¹⁵ presented a method for constructing a singularity-free attitude control system, based on the Euler angles for an AUV, operated at large angles of inclination. This method consists of a hybrid control system using 3-2-1 (yaw, pitch, roll) and 3-2-3 Euler angle sets. The proposed control system is insensitive to problems of singularity and non-uniqueness of Euler angles, and also maintains high quality at all angles of inclination. The performance of the proposed control system at large pitch angles was tested on the nonlinear model of an AUV and its superiority over the approach based on quaternions was demonstrated. Taimuri¹⁶⁻¹⁷ *et al.* investigated a modular mathematical model and a reference technique for the estimation of manoeuvring trajectories and motion time histories of 6 DoF ship motions in deep and shallow waters. Heave, roll and pitch radiation damping are estimated from a unified seakeeping/ manoeuvring time-domain tool using numerical decay tests and implemented in the model. Short waves are idealised by numerical integration along with the vessel's waterline profile and associated hydrodynamic actions are implemented in a response curve format. Hull hydrodynamic forces, derivatives are estimated via semi-empirical methods, CFD or model test data. It is shown that the proposed approach is feasible for the prediction of manoeuvring trajectories of ships and for estimating the ship dynamics before grounding.

In this paper, a mathematical manoeuvring model of an AUV is developed and its dynamics and control are investigated. The AUV is capable of performing a station-keeping manoeuvre in 90° pitch angle orientation after being launched at high speed in horizontal orientation from a parent vehicle. Two different design configurations are investigated, positively buoyant and negatively buoyant. In Section 2, description of 7 DoF manoeuvring motion model, 4 quadrant propeller open water model, rudder/ stern plane model, quaternion model, and Proportional Integral Derivative (PID) control model for propeller revolution are shown. Few model experiment results are also shown in this section. In Section 3, the procedure of optimizing the gain coefficients of the PID controller for the propeller revolution is described and simulation results and discussion about both designs of AUV are shown. The conclusions of this paper are explained in Section 4.

2. MANOEUVRING MATHEMATICAL MODEL OF AUV

A 7 DoF manoeuvring mathematical model for an AUV is used. This model is used for carrying out numerical simulations to predict trajectory, attitude and propeller revolutions of an AUV as it is launched to perform station-keeping manoeuvre in a bow-down orientation. The 6 DoF are for the rigid body dynamics of the AUV and 1 DoF is for propeller rotation variation. The AUV has a cylindrical-shaped body. It is provided with a ducted propeller at the aft. A fixed-pitch Kaplan-type propeller is provided inside the duct¹⁸. The propeller revolution is varied using an electric motor. The AUV is provided with a rudder and stern plane at the aft. The rudder and stern plane are fitted in a cruciform configuration. Both the rudder and stern plane are fixed and cannot be rotated. The rudder and stern plane are fitted in the cruciform configuration because for the subject AUV, depth control and station-keeping manoeuvre is the functional objective as compared to 3D manoeuvring. The size of the rudder/ stern plane is optimized so that they are accommodated within the maximum diameter of the AUV.

The AUV's x_G and x_B are adjusted such that it will tend to pitch bow-down after launching. When the AUV is launched from the parent vehicle, it is in horizontal orientation. The parent vehicle may launch the AUV either at the water surface

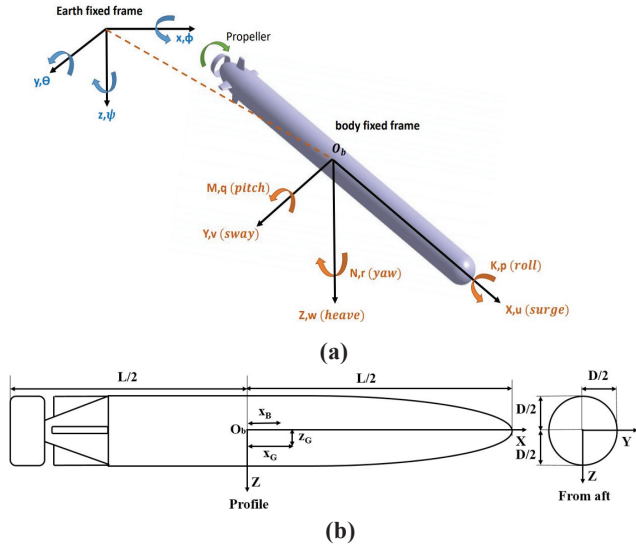
Table 1a. AUV particulars

Particular	Design-I	Design-II
D / L	0.08695	0.08695
Z_d / L	17.3913	43.4782
Z_0 / L	0	21.7391
$U_0 / \sqrt{g * L}$	3.1579	3.1579
$m / (0.5 * \rho * L^3)$	0.0095	0.0099
$B / (0.5 * g * \rho * L^3)$	0.0098	0.0098
x_G / L	0.01478	0.01478
x_B / L	0.00608	0.00608
z_G / D	0.00086	0.00086
z_B / D	0	0
$(x_G - x_B) / L$	0.1	0.1
D_p / D	0.785	0.785
$A_R / L^2, A_F / L^2$ (for each rudder/ stern plane)	0.00119	0.00119
Number of rudders	2	2
Number of stern planes	2	2
C_B	0.8442	0.8442
K_{XX}	0.4D	0.4D
$K_{YY} = K_{ZZ}$	0.25L	0.25L

Table 1b. Prime mover particulars for design-I and design-II for straight running condition

Particular	Case 1	Case 2	Case 3	Case 4
$Q'_E * 10^6$	1.7391	1.0121	0.4561	0.1283
n'_{Max}	3.7311	2.8239	1.8911	0.9711
F'_n	0.8663	0.6498	0.4332	0.2166

or deep inside the water. The initial launch speed is kept high so that the AUV is able to travel as far away as possible from the parent vehicle using the least amount of energy. This is the design objective of the AUV. Due to the method of launching AUV from the parent vehicle, it may also have some roll motion (usually spinning). The propeller rotation is initially controlled using the constant prime mover torque concept. Later, when the AUV pitches bow-down by an angle greater than 70° or the depth of submergence is greater than $10*L$ for design-I and greater than $30*L$ for design-II, a PID controller is activated. The depth sensor and rps feedback are the main components of the controller. The PID controller takes surge acceleration, surge speed, parent vehicle's depth of submergence in water and the propeller revolution as the feedback signal from relevant sensors. Using the feedback signal, the PID controller automatically varies the propeller revolution so that AUV can perform a station-keeping manoeuvre in the bow-down orientation. Trajectory simulations were carried out in the water for launching, followed by 7 DoF motion in the water and finally station-keeping manoeuvre in bow-down condition.


Figure 1. (a) Coordinate system of AUV, and (b) Schematic view of AUV (Not to Scale) .

The simulations were carried out for both design-I and design-II. Design-I is positively buoyant and design-II is negatively buoyant. Since the AUV's pitch angle reaches nearly -90° , quaternion is used instead of Euler angle to avoid singularity during the integration of Euler angular rate in manoeuvring motion simulation. The main particulars of AUV and prime movers are shown in Table 1. The AUV has an axisymmetric design without forward/ aft symmetry. Design iterations were carried out to finalize the values of mass/ buoyancy, dimensions

x_G , x_B , z_G and z_B , ducted propeller and prime mover (torque and rps) selection, the number of straightening fins on propeller duct, optimization of rudder and stern plane area which will enable the AUV to perform desired manoeuvres. The mass and centre of gravity is determined from the AUV's payload and its arrangement.

The schematic view of an AUV and the coordinate system is shown in Fig.1. The 6 DoF manoeuvring equation can be expressed as¹⁹

$$\begin{aligned}
 m[\dot{u} + z_G \dot{q}] &= X_H + X_P + X_F - \\
 m[wq - vr - x_G(q^2 + r^2) + z_G pr] &- (W - B)s\theta \\
 m[\dot{v} - z_G \dot{p} + x_G \dot{r}] &= Y_H + Y_P + Y_F - \\
 m[ur - wp + z_G qr + x_G qp] &+ (W - B)c\theta s\phi \\
 m[\dot{w} - x_G \dot{q}] &= Z_H + Z_P + Z_F - \\
 m[vp - uq - z_G(p^2 + q^2) + x_G rp] &+ (W - B)c\theta c\phi
 \end{aligned} \quad (1a)$$

$$\begin{aligned}
 I_{XX} \dot{p} - mz_G \dot{v} &= K_H - Q_P + K_F + \\
 mz_G(ur - wp) - (z_G W - z_B B)c\theta s\phi & \\
 I_{YY} \dot{q} + m[z_G \dot{u} - x_G \dot{w}] &= M_H + M_P + \\
 M_F - (I_{XX} - I_{ZZ})rp - m[z_G(wq - rv) - x_G(vp - uq)] & \\
 - (x_G W - x_B B)c\theta c\phi - (z_G W - z_B B)s\theta & \\
 I_{ZZ} \dot{r} + mx_G \dot{v} &= N_H + N_P + N_F - \\
 (I_{YY} - I_{XX})pq - m[x_G(ur - wp)] &+ (x_G W - x_B B)c\theta s\phi
 \end{aligned} \quad (1b)$$

When we want to trace the trajectory of the body in space, we need to integrate a set of auxiliary equations. These are expressed as

$$\begin{Bmatrix} \dot{X}_E \\ \dot{Y}_E \\ \dot{Z}_E \end{Bmatrix} = \begin{bmatrix} c\psi & -s\psi & 0 \\ s\psi & c\psi & 0 \\ 0 & 0 & 1 \end{bmatrix} \begin{bmatrix} c\theta & 0 & s\theta \\ 0 & 1 & 0 \\ -s\theta & 0 & c\theta \end{bmatrix} \begin{bmatrix} 1 & 0 & 0 \\ 0 & c\phi & -s\phi \\ 0 & s\phi & c\phi \end{bmatrix} \begin{Bmatrix} u \\ v \\ w \end{Bmatrix} \quad (2)$$

Euler angles (ψ , θ , ϕ) specify the angular relations between the Earth and the body (vehicle) fixed coordinate system. The sequence of rotation followed for coordinate system transfer from Earth to body (vehicle) is (ψ (about Z axis), θ (about new Y axis), ϕ (about new X axis)). The Euler angle rates can be expressed as

$$\begin{Bmatrix} \dot{\phi} \\ \dot{\theta} \\ \dot{\psi} \end{Bmatrix} = \begin{pmatrix} 1 & \sin\phi \tan\theta & \cos\phi \tan\theta \\ 0 & \cos\phi & -\sin\phi \\ 0 & \sin\phi \sec\theta & \cos\phi \sec\theta \end{pmatrix} \begin{Bmatrix} p \\ q \\ r \end{Bmatrix} \quad (3)$$

We also define some additional velocity parameters that can be expressed as

$$U = \sqrt{u^2 + v^2 + w^2}, \quad U_H = \sqrt{u^2 + v^2}, \quad U_V = \sqrt{u^2 + w^2} \quad (4)$$

The drift angle in X-Y plane and attack angle in Y-Z plane can be expressed as

$$\beta = -\tan^{-1}(v/u), \quad \alpha = \tan^{-1}(w/u) \quad (5)$$

The trajectory in Earth fixed coordinate, Euler angles and manoeuvring motion equation are obtained by using the forward Euler integration method can be expressed as

$$[X_E \ Y_E \ Z_E]^T = [X_E \ Y_E \ Z_E]_{t-1}^T + [\dot{X}_E \ \dot{Y}_E \ \dot{Z}_E]_{t-1}^T dt \quad (6)$$

$$[\phi \ \theta \ \psi]^T = [\phi \ \theta \ \psi]_{t-1}^T + [\dot{\phi} \ \dot{\theta} \ \dot{\psi}]_{t-1}^T dt \quad (7)$$

$$[u \ v \ w \ p \ q \ r]^T = [u \ v \ w \ p \ q \ r]_{t-1}^T + [\dot{u} \ \dot{v} \ \dot{w} \ \dot{p} \ \dot{q} \ \dot{r}]_{t-1}^T dt \quad (8)$$

The initial value of the parameters has to be input for this purpose. In the Euler method, the local error is proportional to the square of the step size and the global error is proportional to the step size. The step size (dt) is kept as 0.001 sec. The forward Euler integration method is used to minimize the computation time for feedback control.

In Eqn. (3), there is a well-known singularity at pitch angle (θ) 90° . This is also known as “gimbal lock”. This is usually not a problem for surface ships and submarine manoeuvres. That is because the pitch angle for surface ships and submarines seldom exceeds 50° . However, for AUV simulation, this might become an issue. This is because the AUV needs to carry out a station-keeping manoeuvre in the bow-down orientation. In this orientation, the pitch angle will oscillate around 90° . The above problem in aircraft and spacecraft dynamics is surmounted by using quaternion instead of Euler angles. It is common for the attitude control systems of spacecraft to be commanded in terms of a quaternion. The trajectory integration using the quaternion method will now be described. Before this, a brief introduction to quaternion will be given. Representations of rotations by quaternion are more compact and quicker to compute than the representations by matrices. Unlike Euler angles, the quaternion is not susceptible to “gimbal lock”. For this reason, the quaternion is used in altitude control²⁰. A quaternion is a hyper-complex number with four components^{10,14,21}. A quaternion can be expressed as

$$q_Q = [s_Q, v_Q] \quad (9)$$

Where s_Q is a scalar and v_Q is a 3D vector. If we express the vector in terms of its components, we have the quaternion in an algebraic form that can be expressed as

$$q_Q = [s_Q + x_Q i + y_Q j + z_Q k] \quad (10)$$

where s_Q , x_Q , y_Q and z_Q are real numbers, and i , j , and k are the fundamental quaternion units. The symbols i , j , and k can be interpreted as unit vectors pointing along the three spatial axes. Rotating a point about an axis using a quaternion will now be described. To rotate a point $p_Q(x_Q, y_Q, z_Q)$ through an angle θ_Q about an axis we use the following steps:

1. Convert the point $p_Q(x_Q, y_Q, z_Q)$ to a quaternion,

$$p_Q = [0 + x_Q i + y_Q j + z_Q k]$$

2. Define the axis of rotation as a unit vector,

$$u_Q = [x_{Qu} i + y_{Qu} j + z_{Qu} k]$$

3. Compute the transforming quaternion,

$$q_Q = [\cos(\theta_Q/2), \sin(\theta_Q/2)u_Q]$$

4. Compute the inverse of the transforming quaternion

$$q_Q^{-1} = [\cos(\theta_Q/2), -\sin(\theta_Q/2)u_Q]$$

5. Compute, $p_Q' = q_Q p_Q q_Q^{-1}$

6. Unpack (x_Q', y_Q', z_Q') , $p_Q' = [0 + x_Q' i + y_Q' j + z_Q' k]$

The coordinates of the point $p_Q(x_Q, y_Q, z_Q)$ after the above rotation is $p_Q'(x_Q', y_Q', z_Q')$.

Now we will apply quaternion for the AUV dynamics problem. Here time derivative of quaternion will be required. The quaternion rates are related to body-fixed angular rates²¹ can be expressed as

$$\begin{bmatrix} \dot{q}_{Q0} \\ \dot{q}_{Q1} \\ \dot{q}_{Q2} \\ \dot{q}_{Q3} \end{bmatrix} = \frac{1}{2} \begin{bmatrix} 0 & -p & -q & -r \\ p & 0 & r & -q \\ q & -r & 0 & p \\ r & q & -p & 0 \end{bmatrix} \begin{bmatrix} q_{Q0} \\ q_{Q1} \\ q_{Q2} \\ q_{Q3} \end{bmatrix} + \lambda_Q \begin{bmatrix} q_{Q0} \\ q_{Q1} \\ q_{Q2} \\ q_{Q3} \end{bmatrix} \quad (11)$$

We have the constraint that quaternion shall be of unit value. During numerical integration, the quaternion value may exceed ‘1’ due to drifting. Therefore, normalizing has to be carried out to ensure the unit value of the quaternion. λ_Q is an integration drift correction gain computed can be expressed as:

$$\lambda_Q = 1 - (q_{Q0}^2 + q_{Q1}^2 + q_{Q2}^2 + q_{Q3}^2) \quad (12)$$

We carry out numerical integration using the forward Euler method, as described earlier, to compute the updated quaternion as:

$$\begin{bmatrix} q_{Q0} & q_{Q1} & q_{Q2} & q_{Q3} \end{bmatrix}_t^T = \begin{bmatrix} q_{Q0} & q_{Q1} & q_{Q2} & q_{Q3} \end{bmatrix}_{t-1}^T + \begin{bmatrix} \dot{q}_{Q0} & \dot{q}_{Q1} & \dot{q}_{Q2} & \dot{q}_{Q3} \end{bmatrix}_{t-1}^T dt \quad (13)$$

Euler angles at each time step can be derived from the quaternion can be expressed as:

$$\begin{bmatrix} \phi \\ \theta \\ \psi \end{bmatrix} = \begin{bmatrix} \tan^{-1} \left(2(q_{Q1}q_{Q0} + q_{Q2}q_{Q3}), [1 - 2(q_{Q1}^2 + q_{Q2}^2)] \right) \\ \sin^{-1} \left(2(q_{Q2}q_{Q0} - q_{Q1}q_{Q3}) \right) \\ \tan^{-1} \left(2(q_{Q3}q_{Q0} + q_{Q1}q_{Q2}), [1 - 2(q_{Q2}^2 + q_{Q3}^2)] \right) \end{bmatrix} \quad (14)$$

The question arises of how to find the quaternion at $t = 0$ sec. At $t = 0$ sec, the initial orientation of the body $(\phi_0, \theta_0, \psi_0)$ is known. We write the rotation matrix or the direction cosine matrix can be expressed as

$$H(\phi_0, \theta_0, \psi_0) = \begin{bmatrix} c(\theta)c(\psi) & s(\phi)s(\theta)c(\psi) - c(\phi)s(\psi) & c(\phi)s(\theta)c(\psi) + s(\phi)s(\psi) \\ c(\theta)s(\psi) & s(\phi)s(\theta)s(\psi) + c(\phi)c(\psi) & c(\phi)s(\theta)s(\psi) - s(\phi)c(\psi) \\ -s(\theta) & s(\phi)c(\theta) & c(\phi)c(\theta) \end{bmatrix}_{r=0} \quad (15)$$

The rotation matrix can also be written in terms of a quaternion can be expressed as²⁰

$$H(\phi_0, \theta_0, \psi_0) = \begin{bmatrix} q_{00}^2 + q_{01}^2 - q_{02}^2 - q_{03}^2 & 2(q_{01}q_{02} - q_{03}q_{00}) & 2(q_{01}q_{03} + q_{02}q_{00}) \\ 2(q_{01}q_{02} + q_{03}q_{00}) & (q_{00}^2 - q_{01}^2 + q_{02}^2 - q_{03}^2) & 2(q_{02}q_{03} - q_{01}q_{00}) \\ 2(q_{01}q_{03} - q_{02}q_{00}) & 2(q_{02}q_{03} + q_{01}q_{00}) & (q_{00}^2 - q_{01}^2 - q_{02}^2 + q_{03}^2) \end{bmatrix} \quad (16a)$$

$$H(\phi_0, \theta_0, \psi_0) = \begin{bmatrix} h_{Q11} & h_{Q12} & h_{Q13} \\ h_{Q21} & h_{Q22} & h_{Q23} \\ h_{Q31} & h_{Q32} & h_{Q33} \end{bmatrix} \quad (16b)$$

We can obtain the initial quaternion values can be expressed as

$$q_{00}(0) = 0.5 * \sqrt{(1 + h_{Q11}(0) + h_{Q22}(0) + h_{Q33}(0))}$$

$$\begin{bmatrix} q_{Q1}(0) \\ q_{Q2}(0) \\ q_{Q3}(0) \end{bmatrix} = \frac{1}{4q_{00}(0)} \begin{bmatrix} (h_{Q32}(0) - h_{Q23}(0)) \\ (h_{Q13}(0) - h_{Q31}(0)) \\ (h_{Q21}(0) - h_{Q12}(0)) \end{bmatrix} \quad (17)$$

In Eqn. (17), it can be observed that we shall ensure $q_{00}(0) \neq 0$. There is one more option for determining the $q_Q(0)$. The body-fixed frame can be brought into coincidence with the Earth frame by a single rotation ‘D’ about a fixed axis making angles, A, B, and C with the Earth frame. A, B and C are the direction cosines. The four parameters A, B, C, and D, define the orientation of the body in Earth frame²². We assume that X-axis of the body-fixed frame coincides with the X-axis of the Earth frame at t = 0 sec. This will mean at t = 0 sec, the angles A = B = C = D = 0°. The quaternion at t = 0 sec can be expressed as

$$\begin{bmatrix} q_{00} & q_{Q1} & q_{Q2} & q_{Q3} \end{bmatrix}^T = \begin{bmatrix} \cos\left(\frac{D}{2}\right) & \cos(A)\sin\left(\frac{D}{2}\right) & \cos(B)\sin\left(\frac{D}{2}\right) & \cos(C)\sin\left(\frac{D}{2}\right) \end{bmatrix}^T$$

$$\begin{bmatrix} q_{00} & q_{Q1} & q_{Q2} & q_{Q3} \end{bmatrix}^T = [1 \ 0 \ 0 \ 0]^T \quad (18)$$

By the above method, the orientation of the body and its trajectory in the Earth fixed frame can be determined without any restriction whatsoever.

The hull hydrodynamic forces and moments can be expressed as^{19,23}

$$X_H = X(u) + \frac{\rho L^4}{2} (X'_{qq} q^2 + X'_{rr} r^2) + \frac{\rho L^3}{2} (X'_{uu} \dot{u} + X'_{vr} vr + X'_{wq} wq) + \frac{\rho L^2}{2} (X'_{vv} v^2 + X'_{ww} w^2)$$

$$Y_H = \frac{\rho L^4}{2} (Y'_r \dot{r} + Y'_{pq} pq) + \frac{\rho L^3}{2} (Y'_{ur} |u|r + Y'_v \dot{v} + Y'_{wp} wp) + \frac{\rho L^2}{2} \left\{ Y'_{uv} |u|v + Y'_{v|v|} v \sqrt{(v^2 + w^2)} \right\}$$

$$\frac{\rho}{2} \int_{-\frac{L}{2}}^{\frac{L}{2}} C_D(x) S(x) (v + xr) |v + xr| dx$$

$$Z_H = \frac{\rho L^4}{2} (Z'_q \dot{q} + Z'_{rp} rp) + \frac{\rho L^3}{2} (Z'_{wv} \dot{w} + Z'_{uq} |u|q + Z'_{vp} vp) + \frac{\rho L^2}{2} \left\{ Z'_{uw} |u|w + Z'_{w|w|} w \sqrt{(v^2 + w^2)} \right\}$$

$$\frac{\rho}{2} \int_{-\frac{L}{2}}^{\frac{L}{2}} C_D(x) S(x) (w + xq) |w + xq| dx$$

$$K_H = \frac{\rho L^5}{2} (K'_p \dot{p}) + \frac{\rho L^4}{2} (K'_{up} |u|p) + \frac{\rho \pi}{2} \int_{-\frac{L}{2}}^{\frac{L}{2}} C_{D2}(x) D(x) (R(x)q) |R(x)q| dx$$

$$M_H = \frac{\rho L^5}{2} (M'_q \dot{q} + M'_{rp} rp) + \frac{\rho L^4}{2} (M'_{wv} \dot{w} + M'_{uq} |u|q + M'_{vp} vp) + \frac{\rho L^3}{2} \left\{ M'_{uv} |u|v + M'_{v|v|} v \sqrt{(v^2 + w^2)} \right\}$$

$$\frac{\rho}{2} \int_{-\frac{L}{2}}^{\frac{L}{2}} C_D(x) S(x) (w - xq) |w - xq| (x - x_G) dx$$

$$N_H = \frac{\rho L^5}{2} (N'_r \dot{r} + N'_{pq} pq) + \frac{\rho L^4}{2} (N'_v \dot{v} + N'_{ur} |u|r + N'_{wp} wp) + \frac{\rho L^3}{2} \left\{ N'_{uv} |u|v + N'_{v|v|} v \sqrt{(v^2 + w^2)} \right\} \quad (19)$$

The following modifications are carried out in the Feldman’s model¹⁹ to get the above model. The modulus of surge velocity (|u|) is taken in coefficients involving surge velocity (u). This is because, occasionally, the AUV will have astern velocity, i.e. u < 0. During this time if the absolute value of surge speed is not taken, the damping coefficients will not oppose the motion. During station-keeping manoeuvre surge speed is negligible, i.e. u ~ 0. During this time, in the

Feldman’s model, the roll damping moment becomes 0. This results in large motions of the AUV, as roll excitation due to propeller torque is still present. To overcome this problem, roll moment due to skin friction drag, independent of surge speed, is included in the above model. This ensures roll damping forces and moments for small motions of AUV during the station-keeping manoeuvre. The rudder/ stern plane forces and moment and propeller thrust/ torque model are also modified. It will be described later. Some of the hydrodynamic coefficients were obtained experimentally by conducting angle of attack tests at Naval Science & Technological Laboratory (NSTL), India. The procedure for determining hydrodynamic coefficients of an axisymmetric AUV is already developed²⁴⁻²⁶. Similarly, a procedure for determining added mass coefficients of an ellipsoid of revolution has also been developed²⁷. The same procedure is followed in this paper. For an axisymmetric AUV, the following equations are established²⁴⁻²⁶. The hydrodynamic hull coefficients are shown in Table 2.

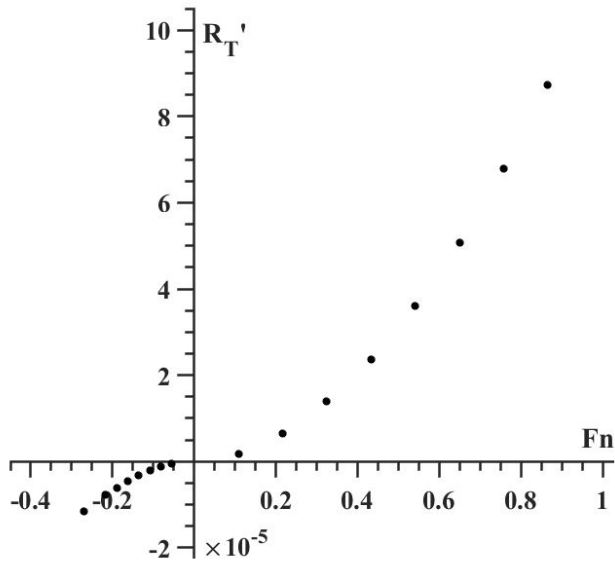
$$\begin{aligned}
 X'_{rr} &= -Y'_r, X'_{qq} = -Y'_q, Z'_w = Y'_v, X'_{vr} = -Z'_w, X'_{wq} = Z'_w, X'_{ww} = X'_{vv}, Y'_{pq} = Y'_p, Y'_{wp} = -Z'_w, \\
 Z'_{uq} &= -X'_{u'}, Z'_{vp} = Z'_w, Z'_{uv} = Y'_{uv}, Z'_{vw} = Y'_{vw}, Z'_{rp} = Y'_r, M'_{uq} = Z'_q, M'_{rp} = (K'_p - M'_q), \\
 M'_{vp} &= Z'_q, N'_{uv} = -M'_{uv}, N'_{ur} = M'_{uq}, N'_{pq} = -(K'_p - M'_q), N'_{vp} = Z'_q, N'_{vw} = M'_{vw}, \\
 Y'_{ur} &= X'_{u'}, Z'_w = Y'_v, Z'_q = -Y'_r, N'_v = -M'_{w'}, N'_r = M'_{q'}
 \end{aligned}$$

The model resistance test results are shown in Fig. 2. The resistance test is carried out for both ahead and astern conditions as the AUV is expected to carry out astern motions also during station-keeping manoeuvre. The experimental results of forces of the bare hull with rotor are also shown in Fig. 2.

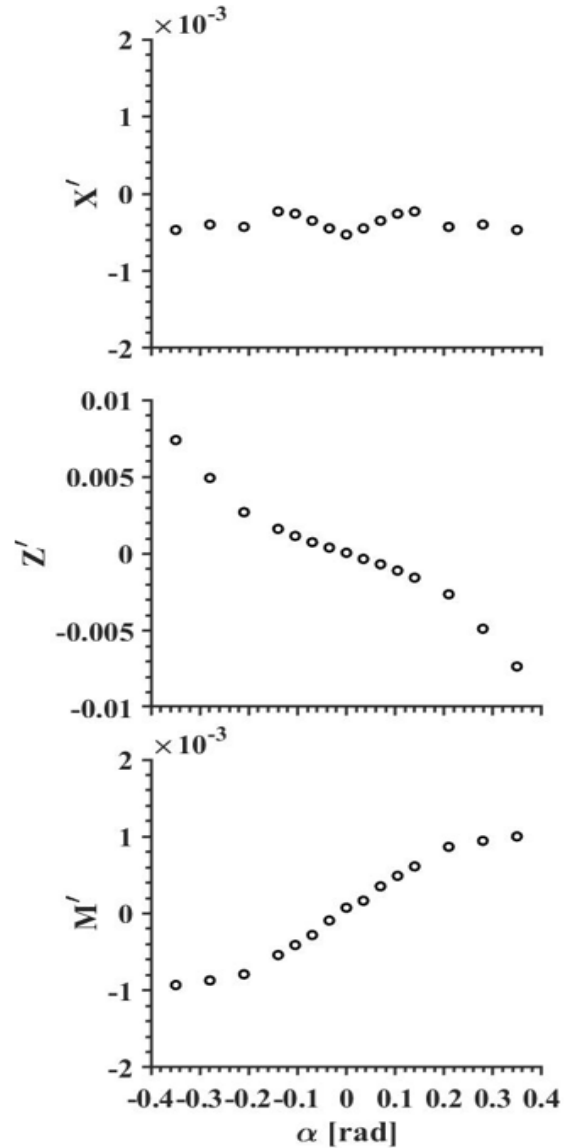
Fixed pitch Kaplan propeller with 19A duct is used for the experiments and simulations. “19A” is a general-purpose duct for application at heavy screw loads. Duct 19A provides about 2% higher efficiency than duct 37¹⁸. Duct 37 presents a better solution when the astern operation is

Table 2. Hydrodynamic hull coefficients

Coefficient	Value	Coefficient	Value
$X'_{u'}$	-0.0001315	$Y'_{v v }$	-0.0484
$Y'_{v'}$	-0.0103	K'_{up}	-0.0000133
$K'_{p'}$	-0.0000122	M'_{uv}	0.0010
$M'_{q'}$	-0.000611	M'_{ww}	0.000
$Y'_{r'}$	0.00029	X'_{vv}	-0.0017
$M'_{w'}$	-0.00118	Y'_{uv}	-0.0137



(a)



(b)

Figure 2. (a) Model resistance test data and (b) Experimental forces: Bare hull + rotor.

Table 3. Details of propeller and propeller-hull interaction coefficients

Coefficient	Value	Coefficient	Value	Coefficient	Value
A_E / A_0	0.7	$\Delta I_{pp} / (0.5 * \rho * L^5)$	$0.25 I_{pp}$	$w_p(ahead)$	0.1416
Z_{pr}	4	$Q_{imbalance}$	$3\% * Q_p$	$w_p(stern)$	0.0
P / D_p	1.2	$t_p(ahead)$	0.12	η_R	1.01
$M_p / (\rho * D_p^3)$	0.0396	$t_p(stern)$	0.4119	η_S	0.98
$I_{pp} / (0.5 * \rho * L^5)$	$8.6821x 10^{-4}$	Straightening vanes on duct	7	η_M	0.93

of interest. The geometrical data of the Ka 4.70 propeller in duct 19A and propeller hull interaction coefficients are shown in Table 3. We used the model corresponding to $P/D_p = 1.2$ for our simulation¹⁸. This is because this pitch ratio is nearest to the optimum design pitch ratio for this AUV. In the downstream side of the duct, straightening vanes are provided to decrease the propeller reaction torque acting on the AUV. The open water results of Ka 4.70, $P/D_p = 1.2$ and Ka 4.70, $P/D_p = 1.27$ (NSTL propeller) are shown in Fig. 3. This figure implies NSTL's propeller has a slightly higher thrust and torque coefficient. Experiments with the NSTL propeller were only carried out for 1st quadrant operation. Wake and thrust coefficients from the experiment for ahead and astern motion are shown in Fig. 4.

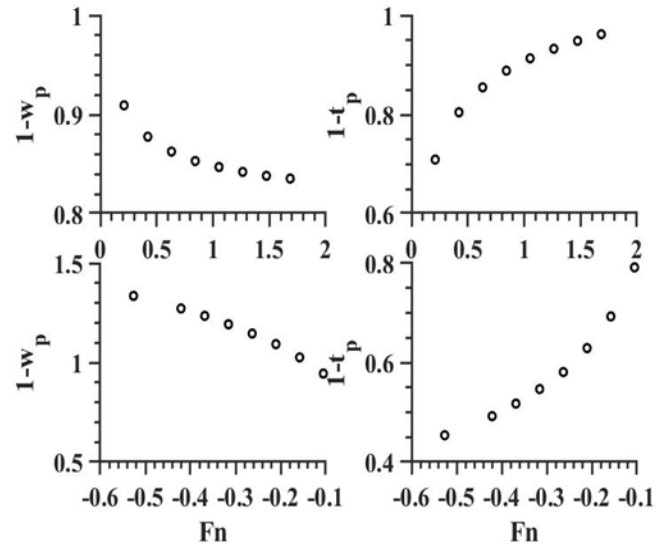


Figure 4. Wake and thrust coefficient from the experiment: ahead (top) and astern (bottom).

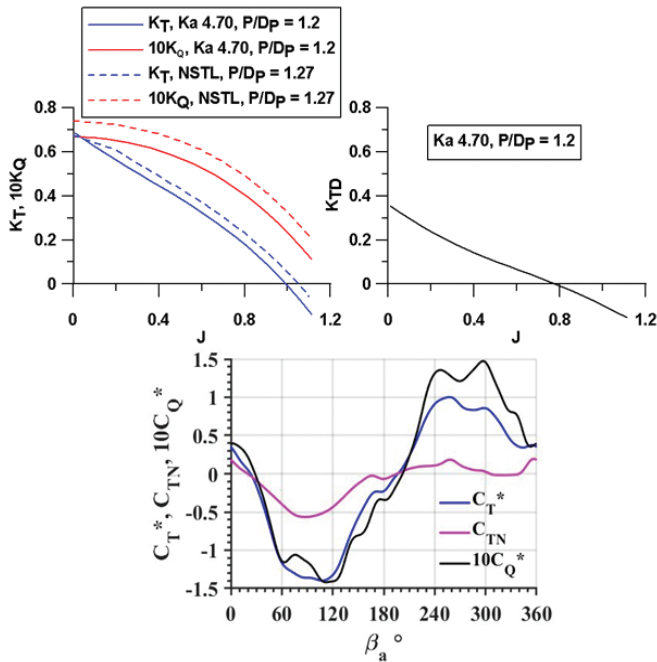


Figure 3. (Top) Open water characteristics of Ka 4.70 propeller¹⁸, and (Bottom) 4 quadrant open water characteristics for Ka 4.70, $P/D_p = 1.2$ propeller¹⁸.

Usually $K_T(J)$, $K_Q(J)$ equations are used for modelling the 1st quadrant open water characteristics of the propeller. For conventional manoeuvring motions, 1st quadrant propeller open water model is sufficient. This is because when manoeuvring in the forward direction, the propeller operates in the 1st quadrant. For some manoeuvring motions, like crash stop astern and crash stop ahead, this is not true. During these manoeuvring motions, the propeller may operate in a quadrant different from the 1st quadrant. During this time, we may require a 4 quadrant propeller open water model. The J , K_T and K_Q coefficients are not suitable for representing the four-quadrant characteristics of a propeller. This is because when $n = 0$ these coefficients become infinite. For the AUV simulation model in this paper, we use 4 quadrant propeller open water model. This is because of two reasons. The first is due to the high initial launch speed (Froude number = 3.1578). At very high speed, when the propeller revolution is less and gradually increasing, it may operate as a turbine or braking condition (high advance coefficient, J). The second reason is when the AUV is carrying out a station-keeping manoeuvre, the propeller may operate in a quadrant different from 1st quadrant. The 4 quadrant propeller thrust and torque model is expressed as

$$\begin{aligned}
 V_a &= (1 - w_p)u \\
 \beta_a &= \text{atan2}(x, y) \text{ where } x = 0.7\pi n D_p \text{ and } y = V_a \\
 X_p &= (1 - t_p) C_T^* (\pi/8) \rho (V_a^2 + (0.7\pi n D_p)^2) D_p^2, \\
 Y_p &= 0, Z_p = 0, M_p = 0, N_p = 0
 \end{aligned} \tag{20a}$$

$$\begin{aligned}
 Q_p &= (1/\eta_R) C_Q^* (\pi/8) \rho (V_a^2 + (0.7\pi n D_p)^2) D_p^3 \\
 C_T^* &= \sum_{k=0}^{20} [A_k^1 \cos(K\beta_a) + B_k^1 \sin(K\beta_a)], \\
 C_Q^* &= \sum_{k=0}^{20} [A_k^2 \cos(K\beta_a) + B_k^2 \sin(K\beta_a)]
 \end{aligned} \tag{20b}$$

The four quadrants of β_a represent the following conditions: First quadrant: $0 \leq \beta_a < 90^\circ$, $V_A > 0$, $n > 0$, Second quadrant: $90^\circ \leq \beta_a < 180^\circ$, $V_A > 0$, $n < 0$, Third quadrant: $180^\circ \leq \beta_a < 270^\circ$, $V_A < 0$, $n < 0$, Fourth quadrant: $270^\circ \leq \beta_a < 360^\circ$, $V_A < 0$, $n > 0$. $\beta_a = 0$ corresponds to the ahead bollard pull condition, i.e. $V_A = 0$, $n > 0$. $\beta_a = 90^\circ$ corresponds to the propeller locked with ship moving ahead, i.e. $V_A > 0$, $n = 0$. $\beta_a = 180^\circ$ corresponds to the astern bollard pull condition, i.e. $V_A = 0$, $n < 0$. $\beta_a = 270^\circ$ corresponds to the propeller locked with ship moving astern, i.e. $V_A < 0$, $n = 0$. The Fourier series coefficients A_k^1 , B_k^1 , A_k^2 , B_k^2 are determined from the open water experiment data. A set of β_a $C_T^*(\beta_a)$, $C_Q^*(\beta_a)$ can be obtained from the open water experiment data. The procedure for computing the coefficients A_k^1 , B_k^1 , A_k^2 , B_k^2 is expressed as

$$\begin{aligned}
 A_k^1 &= (1/2\pi) \int_0^{2\pi} C_T^*(\beta_a) \cos(K\beta_a) d\beta_a, \\
 B_k^1 &= (1/2\pi) \int_0^{2\pi} C_T^*(\beta_a) \sin(K\beta_a) d\beta_a, \\
 A_k^2 &= (1/2\pi) \int_0^{2\pi} C_Q^*(\beta_a) \cos(K\beta_a) d\beta_a, \\
 B_k^2 &= (1/2\pi) \int_0^{2\pi} C_Q^*(\beta_a) \sin(K\beta_a) d\beta_a
 \end{aligned} \tag{21}$$

Where $K = 0, 1, 2, \dots, N$. 'N' depends on the number of experiment data points that are available. It shall be ensured that a sufficient number of experiment data points in all 4 quadrants are available. It can be observed that for determining the Fourier series coefficients, numerical integration is required repetitively. Therefore, some computing tools will help determine the Fourier series coefficients. The four-quadrant characteristics of a Ka 4.70, $P/D_p = 1.2$ propeller are shown in Figure 3. It is usual to plot $10C_Q^*$ as a function

of β_a as their numeral values are lower than that of C_T^* . As the curve is periodic with β_a , it can be expressed as Fourier series. Sufficient number of experiment data points will be required to capture the variation of the curve¹⁸. By writing the 4 quadrant propeller open water equation in C_T^* , C_Q^* and β_a form, the programming becomes very compact and convenient and also error-free. As the AUV will mainly manoeuvre in the vertical plane, the variation in wake fraction will mainly be due to heave and pitch motions. The effective wake fraction at the propeller position during manoeuvring can be computed as²⁸

$$w_p = w_{p0} \exp(C_1 \alpha_p^2) \exp(C_1 \beta_p^2) \tag{22}$$

Where $C_1 = -4.0$. Considering the effects due to the pitch and the roll motion, α_p and β_p are computed as²⁸

$$\begin{aligned}
 \alpha_p &= \alpha + x_p' q' + z_p' p' \\
 \beta_p &= \beta - x_p' r' + z_p' p'
 \end{aligned} \tag{23}$$

The propeller revolution during horizontal manoeuvre keeps varying until the propeller thrust and AUV's drag are balanced. During the horizontal manoeuvre, we consider the propeller revolution variation as²⁹

$$2\pi(I_{pp} + \Delta I_{pp}) \dot{n} + Q_p = \eta_s \eta_M Q_E \tag{24}$$

In the beginning, we consider that the prime mover is working in constant torque operating conditions and the propeller revolution variation is determined from Eq. (24). Thereafter during the station-keeping manoeuvre in the bow-down orientation, the propeller revolution needs to be controlled. Therefore, propeller revolution variation needs to be coupled with AUV dynamics. It is common to use attitude and position in the Earth fixed coordinate system in the control loop for hovering flight control of quadrotor helicopter³⁰ and unmanned helicopter³¹. A similar control scheme is used in this paper. PID control for the propeller revolution for the purpose of station-keeping (depth control) of AUV is written as

$$\Delta n = K_p (u_d - u) + K_D (\dot{u}_d - \dot{u}) + K_I (Z_d - Z) \tag{25a}$$

$$\dot{n} = \Delta n / dt \tag{25b}$$

$$|\dot{n}| \leq 10 \tag{25c}$$

The forward Euler method is used to determine the new propeller revolution

$$n_t = n_{t-1} + \dot{n}_{t-1} dt \tag{26a}$$

$$|n_t| \leq n_{Max} \tag{26b}$$

Here also numerical integration is carried out using the forward Euler method as described earlier with the same time step. A limit is put on the maximum shaft acceleration and shaft revolution to avoid actuator damage. \dot{n} is estimated from Eqn. (25). For vertical station-keeping manoeuvre: $u_d = 0$, $\dot{u}_d = 0$. Outside of the control loop, we keep checking the depth

with feedback from a pressure sensor and activate the propeller revolution control at depth $\sim 10*L$ for design-I and at depth $\sim 30*L$ for design-II with pitch angle $(\theta) > 70^\circ$. The procedure for computing battery capacity will be described. The power at each time instant, total energy and battery capacity can be determined from Eqn. (27). Here also numerical integration is carried out using the forward Euler method as described earlier with the same time step. Each one of the designs of AUV is simulated with four different cases as mentioned in Table 1(b). The battery voltage ($V_{Battery}$) needs to be specified based on motor capacity and other electric items inside the AUV. The unit of power in Eqn. (27a) is in “watts” and that of energy in Eqn. (27b) is in “watt-seconds”. The ampere-hour capacity of the battery can be determined as shown in Eq. (27c). We divide by 3600 in Eqn. (27c) to convert seconds to hours. Power and energy determined here are only for the propeller’s prime mover operation.

$$Power = 2\pi n Q_E \quad (27a)$$

$$Energy_t = Energy_{t-1} + Power * dt \quad (27b)$$

$$Battery\ capacity\ (ampere\ -\ hour) = Total\ Energy / (3600 * V_{Battery}) \quad (27c)$$

The procedure for optimizing the gain coefficients will be described. We define the cost function as

$$J_{cost} = Energy / D_E \quad (28)$$

Here Energy is the total energy consumed till the end of the station-keeping manoeuvre. We want that the AUV shall travel maximum distance from the parent body consuming minimum energy. We intend to make the cost function minimum. The gain coefficient giving the minimum cost function is selected. We vary the gain coefficients (incremented in the interval of 0.1) in the range as

$$K_p : (0.1 \sim 10), K_D : (0.1 \sim 10), K_I : (0.1 \sim 10) \quad (29)$$

The rudder and stern plane model is used. The force and moment due to rudder at AUV’s centre of gravity are computed as²⁸

$$\begin{aligned} X_R &= -F_{NR} \sin(\delta_R), & Y_R &= -(1+a_H)F_{NR} \cos(\delta_R) \\ N_R &= -(1+a_H)x_R F_{NR} \cos(\delta_R), & K_R &= -(1+a_H)z_R F_{NR} \cos(\delta_R) \end{aligned} \quad (30)$$

The rudder normal force can be computed as

$$F_{NR} = \rho C_R (\lambda_R) A_R U_R^2 \sin(\alpha_R) / 2 \quad (31)$$

The above parameters are estimated as

$$C_R (\lambda_R) = 6.13 \lambda_R / (\lambda_R + 2.25)$$

$$U_R = (1-w_R) \sqrt{(u_R^2 + v_R^2)}$$

$$u_R = (1-w_R)u, \quad v_R = -\gamma_R (v + l_R r - z_R p), \quad l_R = 2x_R, \quad \alpha_R = -atan2(v_R, u_R) \quad (32)$$

Here $\delta_R = 0$ as the rudder is fixed. As the rudder is in front of the propeller, the propeller slipstream does not affect inflow velocity to the rudder. Since the rudder is

in the wake of the main hull and is located within the diameter of the main hull, the value of w_R is taken as 0.1. The force and moment due to the stern plane at AUV’s centre of gravity are computed as

$$\begin{aligned} X_F &= -F_{NF} \sin(\delta_F), & Z_F &= -(1+a_H)F_{NF} \cos(\delta_F), \\ M_F &= -(1+a_H)x_F F_{NF} \cos(\delta_F) \end{aligned} \quad (33)$$

The stern plane normal force can be computed as

$$F_{NF} = \rho C_F (\lambda_F) A_F U_F^2 \sin(\alpha_F) / 2 \quad (34)$$

The parameters in the above equation are estimated as

$$C_F (\lambda_F) = 6.13 \lambda_F / (\lambda_F + 2.25)$$

$$U_F = (1-w_F) \sqrt{(u_F^2 + v_F^2)}$$

$$\begin{aligned} u_F &= (1-w_F)u, & v_F &= -\gamma_F (w - l_F q - z_R p), \\ l_F &= 2x_F, & \alpha_F &= -atan2(v_F, u_F) \end{aligned} \quad (35)$$

Here $\delta_F = 0$ as the stern plane is fixed. As the stern plane is in front of the propeller, the inflow velocity to the stern plane is not affected by the propeller slip stream. Since the stern plane is in the wake of the main hull and is located within the diameter of the hull, the value of w_F is taken as 0.1. We assume $a_H = 0.5$, $\gamma_R = \gamma_F = 0.8$.

3. AUV SIMULATION AND VALIDATION

The variation of the cost function with PID controller gains for design - I and II for different maximum prime mover torque are shown in Fig. 5. The optimal gain coefficients are those which have the least cost function. Hence, gain coefficients corresponding to a blue area in Figure 5 are selected. It may be observed that after a certain numerical value of gain coefficients, there is no significant change in colour. This is because of the limiter used in the model, see Eqn. (26). After a certain value of the gain coefficient, the limiter, shown in Eqn. (26), overrides the feedback control command signal. For Case 4 of both the designs, PID gain coefficients are not shown because the controller cannot maintain the required depth in given time due to less prime mover power.

The output of the numerical simulation for design-I is as shown in Fig. 6. AUV moves about 18.25L, 18*L and 18*L away from the parent vehicle for Case 1, Case 2 and Case 3 respectively as it starts station-keeping manoeuvre. For all the three cases the AUV is able to maintain the desired station-keeping depth. In Case 4, AUV is unable to reach desired station-keeping depth in a given time and is about 7*L away from the parent vehicle. The output of numerical simulation for design-II is as shown in Figure 7. AUV moves about 23.5*L, 23.75*L and 24*L away from the parent vehicle for Case 1, Case 2 and Case 3 respectively as it starts station-keeping manoeuvre. In Case 4, AUV is unable to do station-keeping at 43.47*L depth and keeps sinking into the water. This is because the propeller revolution has reached its limit. As the propeller is working in astern condition, the astern thrust generated is not sufficient to overcome the negative buoyancy of the AUV. Due to the positive surge speed, the hydrodynamic damping

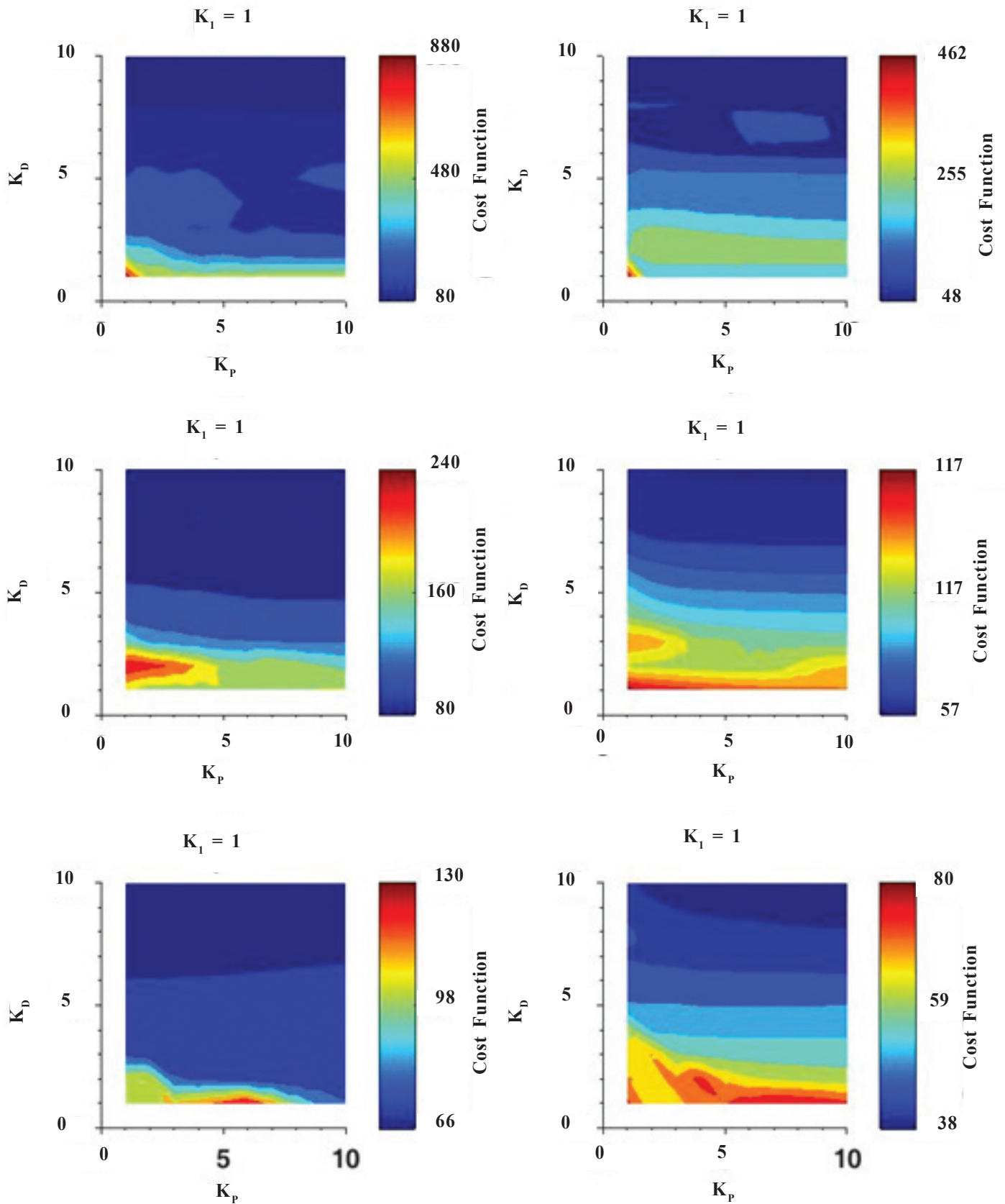


Figure 5. Variation of a cost function for different gain coefficients for design-I (Left) and design-II (Right). Top row: Case 1, Middle row: Case 2, Bottom row: Case 3.

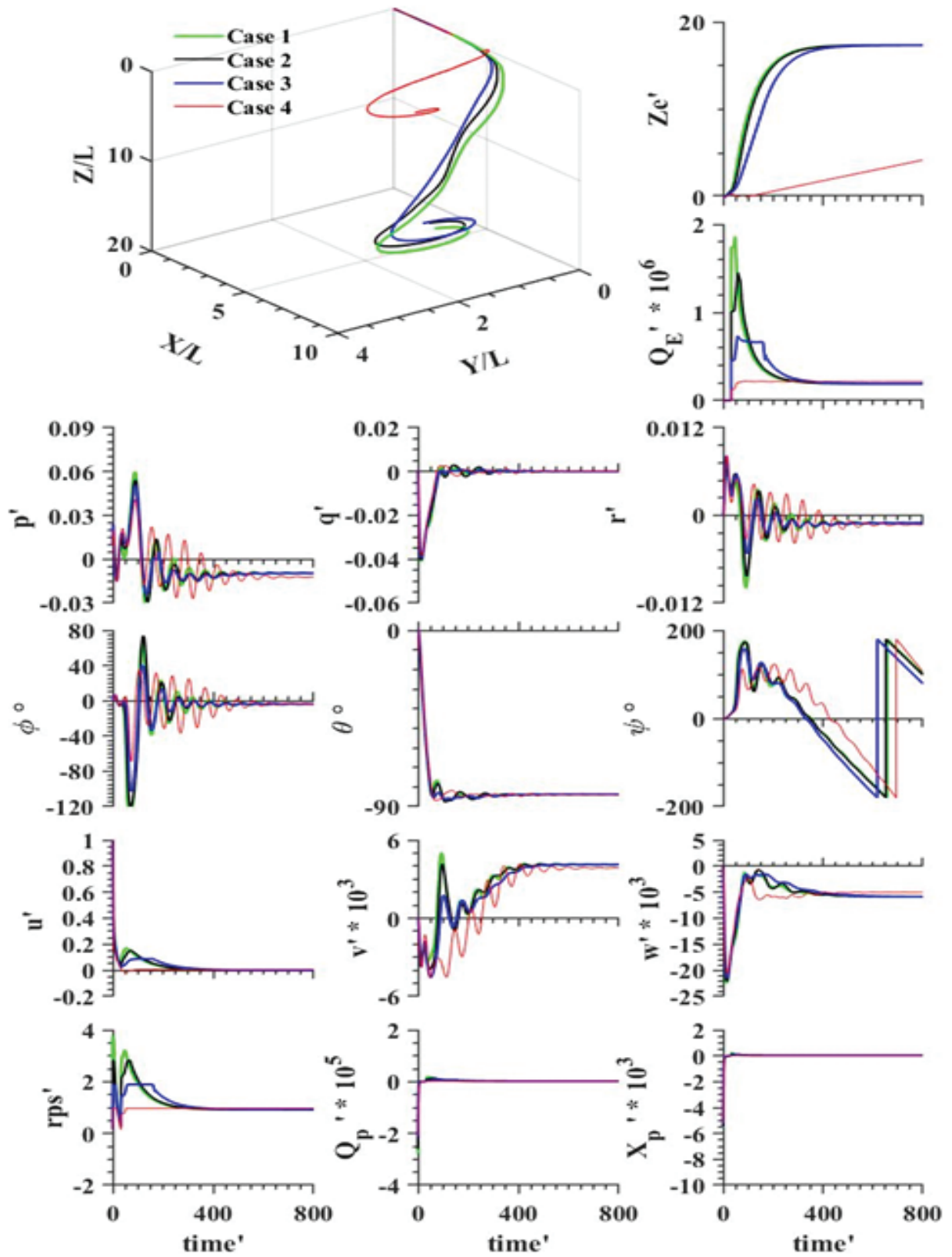


Figure 6. Variation of AUV dynamics and trajectory for design-I.

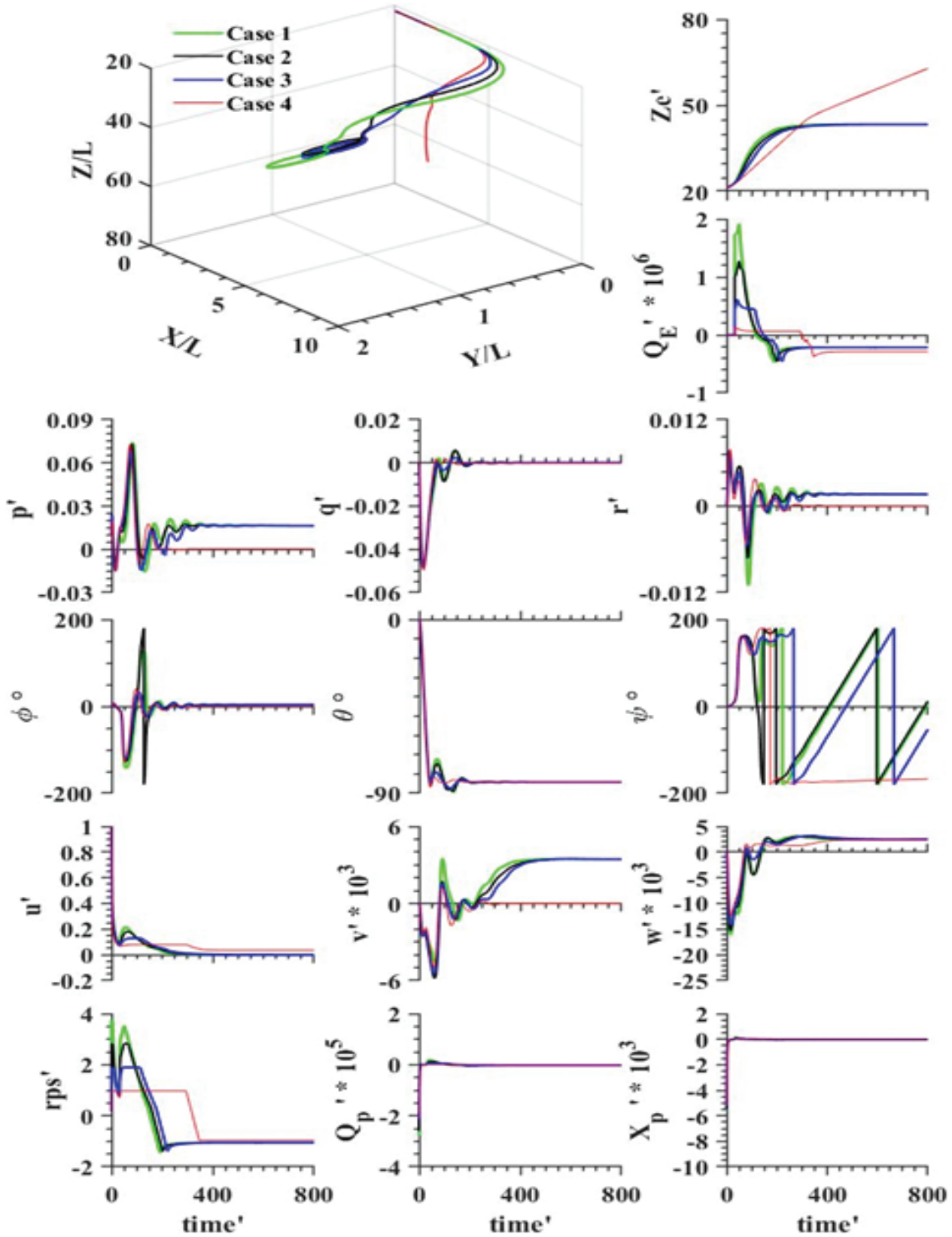


Figure 7. Variation of AUV dynamics and trajectory for design-II.

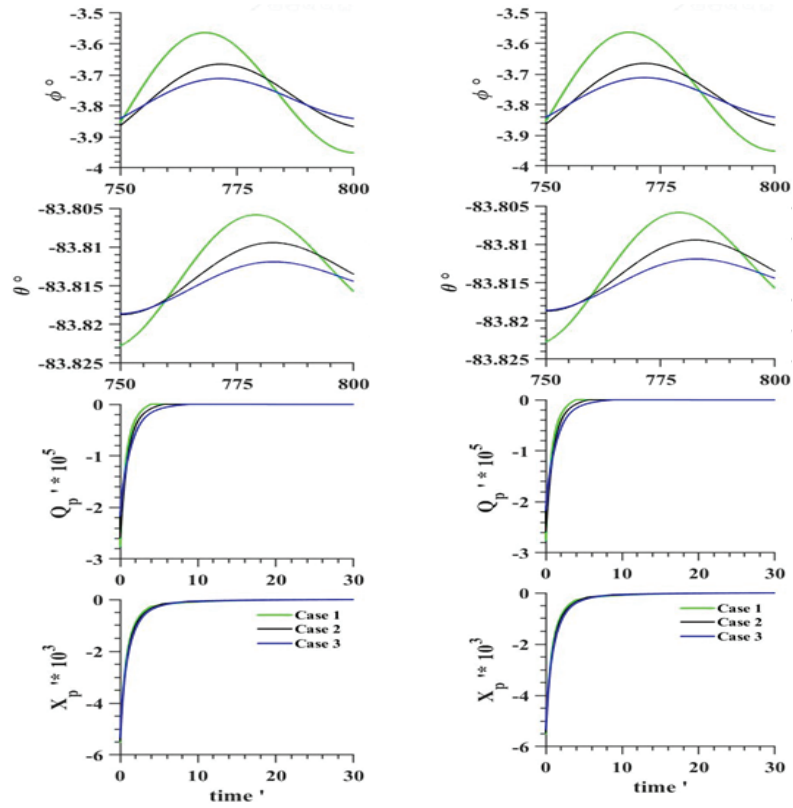


Figure 8. Magnified view of the variation of Euler angles and propeller thrust/ torque for design-I (Left) and design-II (Right).

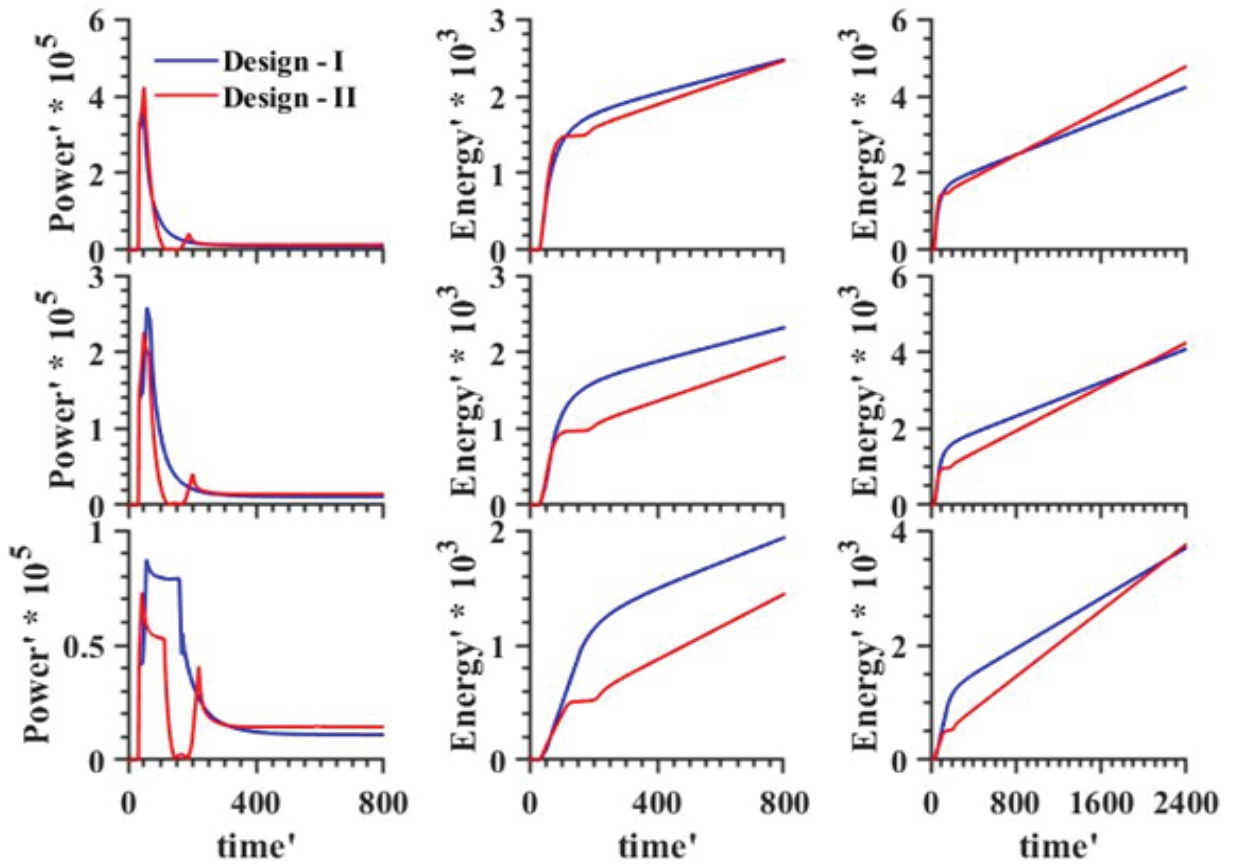


Figure 9. Comparison of power (first column) and energy (second and third column) for design-I and design-II. Top row: Case 1, Middle row: Case 2, Bottom row: Case 3.

Table 4. Optimal gain coefficients

	Design-I			Design-II		
	Case 1	Case 2	Case 3	Case 1	Case 2	Case 3
K_p	8.3	6.7	3.2	6.8	6.7	3.8
K_D	9.1	7.6	7.4	8.3	8.7	9.2
K_I	1	1	1	1	1	1
Cost Function	81.07	81.00	66.88	48.60	57.98	37.69
$(Z_d - Z_0)/L$	17.4	17.4	17.4	21.73	21.73	21.73

forces and moments decrease the other dynamics of the AUV. Interestingly this situation does not happen for design-I case 4. This is because there the propeller is working in forward condition and the forward thrust generated is sufficient to overcome the positive buoyancy of the AUV.

For designs-I and II, the variation of Euler angles (φ and θ) towards the end of the manoeuvre and the variation of propeller thrust and torque at the beginning of the manoeuvre is shown in Fig. 8. The variation is only shown for case 1, 2 and 3 in which AUV is controllable. It can be observed that Euler angles undergo small amplitude oscillations even after AUV dynamics have stabilized. The propeller thrust and torque is negative for a short time. During this time the propeller works as a turbine. For both designs-I and II, the AUV pitches bow down in very short time. Therefore, the time taken to attain station keeping depth is more than the time required for horizontal travel. Consequently, the distance from the parent vehicle is higher in depth direction as compared to horizontal direction. Initially, as the launch speed is high and the propeller rotation is increasing, due to the high advance coefficient, the propeller operates as a turbine or in braking condition. This tends to give a large negative thrust. This decelerates the AUV in water. The thrust bearing shall be capable of taking loads in both ahead/ astern directions. Due to the high launch speed, a minimum prime mover power is necessary so that forward thrust is generated during the initial manoeuvring stage. The propeller revolution is continually varying during launching and stabilizes during station-keeping manoeuvre. During station-keeping manoeuvre in bow-down condition, there is no restoring or stiffness term for rolling and yawing motion while restoring or stiffness term is present for pitching motion. Therefore, during station-keeping manoeuvre, only pitch rate is damped while small roll and yaw rate is present. A small roll excitation is present due to the rotation of the propeller. During the station-keeping manoeuvre, in design-I propeller revolution is positive, while in design-II it is negative. Therefore, roll excitation due to the propeller causes a negative roll rate for design-I and positive roll rate in design-II. Due to the coupling of the dynamics, the yawing rate becomes negative for design-I and positive for design-II. For design-I, during station-keeping manoeuvre, for all the cases the propeller has to only overcome the positive buoyant force.

Therefore, the propeller rotation stabilizes to the same positive value resulting in the same steady roll and yaw rate for all the cases. The situation is reversed in the case of design-II. Here for all the cases, the propeller has to overcome the negative buoyant force. Therefore, the propeller rotation stabilizes to the same negative value. The steady roll and yaw rate are same for all the cases but opposite to design-I. In summary, the final AUV dynamics during the station-keeping manoeuvre is due to the roll moment induced by propeller reaction torque. In actual conditions, due to waves/currents prevalent in the ocean, their influence during station-keeping manoeuvre may be important. This is because there is very less damping and no restoring term for roll and yawing motion.

The desired station-keeping depth can be achieved by the PID controller by selecting proper gain (K_p , K_I and K_D) coefficients. The optimal gain coefficients for design-I and design-II are shown in Table 4 for non dimensional operating time of 800. It can be seen that with an optimum prime mover power the mission objectives can be achieved for both designs-I and II. It is seen that cost function values are higher for design-I as compared to design-II. This happens even though the difference in desired depth is higher for design-II as compared to design-I. This is because net buoyancy force $|W - B|$ for design-I is higher than design-II. Therefore, the propeller needs to produce higher forward thrust. However, the energy consumed for design-I and design-II also varies with time duration of manoeuvring. The variation of the prime mover power and energy for both the designs is shown in Fig. 9. For longer time duration of manoeuvring, design-II consumes higher energy than design-I. This happens even though in design-II, the net buoyancy force is less and the propeller produces lower thrust. The reason is, in design-II propeller works in astern thrust condition and its efficiency is lower. In design-II, for some time duration ($t^* = 100 \sim 200$), the propeller works as a turbine. The propeller rotates the propulsion motor during this period. Therefore, there is no increment in the energy consumed during this period. Similarly, for initial few seconds after launching (Figure 8), in design-I and design-II the propeller works as a turbine. The electrical components and the battery capacity of the AUV, needs to be designed for such operating condition.

4. DISCUSSION AND CONCLUSIONS

In this paper, a methodology for automatic control of propeller revolution for performing station-keeping manoeuvre in nearly 90° bow down orientation of an AUV is demonstrated. The AUV is launched at high speed from a parent vehicle in horizontal orientation. For this purpose, a 7 DoF manoeuvring model of AUV is used. In the mathematical model, 4 quadrant propeller open water model, quaternion for computing AUV's orientation, prime mover torque/ shaft revolution characteristics are incorporated. The objective is to avoid singularities in the conventional manoeuvring mathematical model and control propeller revolution, in ahead and astern direction motion, to achieve a station-keeping manoeuvre. The main conclusions of this paper are as follows:

1. PID type controller for the propeller revolution works well in station-keeping manoeuvre in the bow-down orientation. The hull, propeller and prime mover characteristics are required to compute the optimal gain coefficients for the PID controller for the propeller revolution. These parameters also influence the trajectory, attitude and dynamics of the AUV. It is shown that an optimum prime mover power is necessary to achieve the design objectives.
2. When the AUV is in the bow-down orientation, the hydrostatic restoring term for rolling and yawing becomes negligible. The propeller revolution in this condition is lower as it is used for performing station-keeping manoeuvres, therefore the reaction torque acting on the AUV is also lower. However, as the rudder and stern plane and main hull roll damping are less, the AUV still undergoes spinning about the longitudinal axis. Due to 7 DoF motion coupling and the absence of a hydrostatic restoring term in yawing motion, AUV undergoes yawing motion also. Only the pitching motion of AUV gets damped due to the hydrostatic restoring term.
3. The energy consumed for achieving orientation for station-keeping manoeuvre depends both on the AUV design and also the time duration of manoeuvre. The propeller for short durations during this manoeuvre may work as a turbine. The propulsion motor, battery capacity and the associated systems needs to be designed considering these aspects.
4. Free running prototype trials have to be carried out at sea for validation. These are costly and require planning and effort. This is part of our future work.

REFERENCES

1. Li, J.H.; Yoon, B.H.; Oh, S.S.; Cho, J.S. & Kim, J.G. Development of an intelligent autonomous underwater vehicle, P-SURO. Ocean IEEE Sydney. Published online 2010:1-5. doi:10.1109/OCEANSSYD.2010.5603593.
2. Song, L.; Zhang, H.; Liu, Y.; Wang, Y. & Yang, Y. Research on negative-buoyancy autorotating-rotor autonomous underwater vehicles. *Appl. Ocean. Res.*, 2020, **99**(4), 102123. doi:10.1016/j.apor.2020.102123.
3. Rezazadegan, F.; Shojaei, K.; Sheikholeslam, F.; Chatraei, A. A novel approach to 6-DOF adaptive trajectory tracking control of an AUV in the presence of parameter uncertainties. *Ocean Eng.*, 2015, **107**, 246-258. doi:10.1016/j.oceaneng.2015.07.040.
4. Ayyangar, V.B.S.; Krishnankutty, P.; Korulla, M. & Panigrahi, P.K. Stability analysis of a positively buoyant underwater vehicle in vertical plane for a level flight at varying buoyancy, BG and speeds. *Ocean Eng.* 2018, **148**(11), 331-348. doi:10.1016/j.oceaneng.2017.11.030.
5. Rodriguez, J.; Castañeda, H.; Gordillo, J.L. Lagrange modeling and navigation based on quaternion for controlling a micro AUV under perturbations. *Rob. Auton. Syst.*, 2020, **124**, 103408. doi:10.1016/j.robot.2019.103408.
6. Ferreira, B.; Pinto, M.; Matos, A.; Cruz, N.; Deec F. Control of the MARES Autonomous Underwater Vehicle. In OCEANS 2009, MTS/IEEE Biloxi - Marine Technology for Our Future: Global and Local Challenges. *IEEE*, 2009. doi:10.23919/OCEANS.2009.5422133.
7. Ferreira, B.M.; Jouffroy, J.; Matos, A.C.; Cruz, N.A. Control and guidance of a hovering AUV pitching up or down. Ocean 2012 MTS/IEEE Harnessing Power Ocean. Published online 2012. doi:10.1109/OCEANS.2012.6405081.
8. Chen, C.W.; Kouh, J.S.; Tsai, J.F. Maneuvering modeling and simulation of AUV dynamic systems with Euler-Rodriguez quaternion method. *China Ocean Eng.* 2013, **27**(3), 403-416. doi:10.1007/s13344-013-0035-7.
9. Fjellstad, O.E.; Fossen, T.I. Quaternion Feedback Regulation of Underwater Vehicles. In Proceedings of the 3rd IEEE Conference on Control Applications. 1994, 857-862. doi:10.1109/CCA.1994.381209
10. Andersen, T.S.; Kristiansen, R. Quaternion Path-Following in Three Dimensions for a Fixed-Wing UAV Using Quaternion Blending. 2018 IEEE Conf. Control Technol. Appl. CCTA 2018. Published online 2018, 1597-1602. doi:10.1109/CCTA.2018.8511510
11. Chen, P.; Guan, T.; Zhang, G.; Shi, S.; Shen, J.; Yuan, M. Three dimensional stabilization controller based on improved quaternion transformation for fixed-wing UAVs. *ISA Trans.* 2021;(xxxx). doi:10.1016/j.isatra.2021.10.035
12. Wang, R.; Liu, J. Trajectory tracking control of a 6-DOF quadrotor UAV with input saturation via backstepping. *J. Franklin Inst.* 2018, **355**(7), 3288-3309. doi:10.1016/j.jfranklin.2018.01.039
13. Li, Y.; Li, Y.; Wu, Q. Design for three-dimensional stabilization control of underactuated autonomous underwater vehicles. *Ocean Eng.* 2018, **150**(1), 327-336. doi:10.1016/j.oceaneng.2017.12.071
14. Lekkas, A.M.; Fossen, T.I. A quaternion-based LOS guidance scheme for path following of AUVs. In IFAC Proceedings Volumes (IFAC-PapersOnline). Vol 9. IFAC; 2013:245-250. doi:10.3182/20130918-4-JP-3022.00070.
15. Gavrilina, E.; Chestnov, V. Singularity-Free Attitude Control of the Unmanned Underwater Vehicle. In 24th International Conference on System Theory, Control and Computing, ICSTCC 2020 - Proceedings. 2020, 512-519.

- doi:10.1109/ICSTCC50638.2020.9259733
16. Taimuri, G.; Mikkola, T.; Matusiak, J.; Kujala, P.; Hirdaris, S. The Influence of Hydrodynamic Assumptions on Ship Maneuvering. *NuTTS 2019*. Published online 2019, **6**. doi:10.6084/m9.figshare.10185065.
 17. Taimuri, G.; Matusiak, J.; Mikkola, T.; Kujala, P.; Hirdaris, S. A 6-DoF maneuvering model for the rapid estimation of hydrodynamic actions in deep and shallow waters. *Ocean Eng.* 2020, **218**, 108103. doi:10.1016/j.oceaneng.2020.108103.
 18. Carlton, J.S. *Marine Propellers and Propulsion*. Third. Elsevier publication Ltd; 2010. doi:10.1016/B978-0-08-097123-0.01001-7.
 19. Feldman, J. *DTNSRDC Revised Standard Submarine Equations of Motion*; 1979.
 20. Vince, J. *Mathematics for Computer Graphics* Springer, London; 2010. doi:10.1007/978-3-642-83539-1_16.
 21. Cooke, J.M.; Zyda, M.J.; Pratt, D.R.; McGhee, R.B. NPSNET: Flight Simulation Dynamic Modeling using Quaternions. *Presence*. 1992, **1**(4), 404-420. doi:10.1162/pres.1992.1.4.404.
 22. Rolfe, J.M.; Staples K.J. *Flight Simulation*. Cambridge Aerospace Series, 1988.
 23. Gertler, M.; Hagen, G.R. Standard equations of motion for submarine simulation. Published online 1967, **42**. doi:10.21236/ad0653861.
 24. Renilson, M. *Submarine Hydrodynamics*, 2015. doi:10.1007/978-3-319-16184-6.
 25. Prestero, T. Verification of a six-degree of freedom simulation model for the REMUS autonomous underwater vehicle. Published online 2001. doi:10.1575/1912/3040.
 26. Rasekh, M. & Mahdi, M. Combining CFD, ASE, and HEKF approaches to derive all of the hydrodynamic coefficients of an axisymmetric AUV. *Proc. Inst. Mech. Eng. Part M J. Eng. Marit. Environ.* Published online 2021. doi:10.1177/14750902211034361.
 27. Korotkin, A.I. *Added Masses of Ship Structures*. 1st ed. Springer, Dordrecht, 2007. doi:10.1007/978-1-4020-9432-3
 28. Hirano, M.; Takashina, J. *Ship Maneuverability - Theory and Its Application*. Mitsui Akishima Research Laboratory, 2010.
 29. Patil, P.V.; Prabu, C.S.K.; Nagarajan, V.; Sha, O.P. Numerical simulation of ship navigation in rough seas based on ECMWF data. *Brodogradnja*. 2021, **72**(1), 19-58. doi:10.21278/brod72102.
 30. He, Z.; Zhao, L. A simple attitude control of quadrotor helicopter based on Ziegler-Nichols rules for tuning pd parameters. *Sci. World J.* 2014;2014. doi:10.1155/2014/280180.
 31. Khizer, A.N.; Yaping, D.; Amjad Ali, S.; Xiangyang, X. Stable hovering flight for a small unmanned helicopter using fuzzy control. *Math Probl. Eng.* 2014;2014. doi:10.1155/2014/208253.

CONTRIBUTORS

Mr Prasad Vinayak Patil is a PhD student at Ocean Engineering and Naval Architecture Department, IIT Kharagpur, India. He carried out the implementation of the algorithm, the simulation in MATLAB and overall analysis of the work.

Mr Md. Kareem Khan is a Scientist E at Naval Science & Technological Laboratory, Visakhapatnam, India. He is responsible for carrying out all the experiments, collecting the experiment data and its post-processing.

Dr Manu Korulla is a Scientist G at Naval Science & Technological Laboratory, Visakhapatnam, India. She arranged for resources for conducting experiments and provided inputs for carrying out the experiments and analysing the results.

Dr Vishwanath Nagarajan is an Associate Professor at Ocean Engineering and Naval Architecture Department, IIT Kharagpur. He carried out the formulation of the problem statement for the study, the definition of the constraints, requirements.

Prof Om Prakash Sha is a Professor at Ocean Engineering and Naval Architecture Department, IIT Kharagpur. He provided inputs towards the overall aim and objectives of the work, its methodology, and its implementation.